

Study on Kerosene-submerged Jet Electrochemical Machining and Optimization of the Electrochemical Machining Parameters

Xinchao Li, Pingmei Ming*, Xinmin Zhang*, Shen Niu, Xingshuai Zheng, Liang Yan, Wei Wang, Yunyan Zhang

Institute of Non-traditional Machining & Equipment, Henan Polytechnic University, Jiaozuo, 454000, China

*E-mail: mingpingmei@163.com, hpuzxm@163.com

Received: 24 September 2020 / *Accepted:* 9 November 2020 / *Published:* 30 November 2020

Kerosene-submerged jet electrochemical machining (Jet-ECM) has been proven to be an effective process to enhance the machining localization of Jet-ECM. However, this process can only show its best capabilities and advantages under appropriate electrochemical machining parameters. Its machining effects will be weakened when the workpiece surface is relatively large or electrolytic products generated during machining are quite more, which may cause the electrolyte and electrolytic products to accumulate on the workpiece surface, thereby affecting its mass transfer environment. Therefore, for further improving its process capabilities, it is necessary to eliminate the accumulation of electrolyte and electrolytic products on the workpiece surface. And thus, this paper focuses on optimizing its electrochemical machining parameters and investigating the surface effect and shape effect of the workpiece on its machining localization and machining accuracy experimentally and theoretically. It was found that the surface effect and shape effect of the workpiece has a significant influence on its machining localization and machining accuracy. And kerosene medium instead of air medium surrounding the electrolyte-jet can improve the machining localization of Jet-ECM. Besides, compared with traditional Jet-ECM, kerosene-submerged Jet-ECM can produce high accuracy microstructure with a smooth surface. Additionally, micro-sized features fabricated by Jet-ECM on the small surface flat workpiece and curved surface workpiece feature higher machining accuracy and better surface quality than the large surface flat workpiece.

Keywords: Kerosene-submerged jet electrochemical machining; machining localization; machining accuracy; surface effect; shape effect

1. INTRODUCTION

Electrochemical machining (ECM) is a non-traditional machining technology, which can fabricate microstructures by anodically dissolving metallic workpiece material atom by atom. It demonstrates attractive application potential in manufacturing hard-to-cut metallic materials because

of its inherent advantages including almost no limitation in workpiece material mechanical performances, no wear of the cathode tool, no formation of the re-casted layer and cracks, and excellent surface quality, etc. Jet electrochemical machining (Jet-ECM) is a unique form of electrochemical machining process, which utilizes the electrolyte-jet as the cathode tool to electrochemically fabricate desired metallic microstructures cost-effectively and flexibly. In addition to the inherent advantages of ECM process, Jet-ECM process also features higher machining selectivity, larger material removal rate (MRR) and greater operating flexibility.

Jet-ECM has been used to fabricate various micro-sized features including micro-dimple [1], micro-hole [2], micro-groove [3], 3D complex microstructure [4], and surface texture [5] by controlling the movement path of the electrolyte-jet and electrochemical machining parameters. However, the dimensional accuracy and surface quality of these machined microstructures are still undesirable to satisfy the requirements of engineering applications due to its relatively low machining localization. Therefore, further improving its machining localization has been a research focus, which has been intensively investigated by the researchers. Sen and Shan [6] studied the effect of machining parameters including machining voltage, electrolyte concentration and feed rate of the cathode nozzle on the radial overcut and taper of the hole manufactured by Jet-ECM, and they found that increasing the feed rate of the cathode nozzle can reduce them significantly, and thus improve its machining localization. Yu et al. [7] found that pulsed electrolyte-jet machining can reduce the machined holes' taper and improve their surface quality, thereby improving its machining accuracy. Mitchell-Smith et al. [8] reported that the addition of sodium iodide (NaI) into the commonly used sodium nitrate (NaNO_3) electrolyte enables to enhance the dimensional accuracy of the micro-dimples machined by Jet-ECM. Thanigaivelan et al. [9] found the use of acidified electrolyte can improve the machining localization of Jet-ECM since the acidified electrolyte can facilitate the removal of electrolytic products from the machining gap. However, the acidified electrolyte has the potential risk to cause an environmental pollution problem, which requires higher equipment development and maintenance costs. Therefore, this reduces, to some extent, the applicability of the Jet-ECM process. Zhang et al. [10] investigated the influence of the orientations of the jet on the machining accuracy of the Jet-ECM, and they found that Jet-ECM with a horizontal jet can obtain high accuracy microstructures with smooth surface quality.

To better improve the machining localization and machining accuracy of Jet-ECM, scholars conducted a lot of theoretical research and exploration. Kozak et al. [11] presented a theoretical model to describe the distribution characteristic of electric field and studied the influence of variation of electrolyte conductivity on the process performance. Hackert and his co-workers [12, 13] conducted a series of numerical simulation studies on the Jet-ECM, and they found that a secondary electric contact phenomenon occurred between the anode workpiece and cathode nozzle caused by the reflected electrolyte, which can reduce its machining localization. Mitchell-Smith et al. [14] developed a two-dimensional (2D) simulation model to analyze the effect of cathode nozzle tip shape on the profile of machined microstructures. Their later work [15] investigated the effect of the incident angle of the electrolyte-jet on the resultant geometric profile and surface finish of the machined groove. Furthermore, Wang et al. [16] examined the interrelation between the shape of the jet, machining parameters, and groove edges conditions in jet electrochemical milling grooves, and they demonstrated

stray corrosion on the grooves edges is able to be significant reduced by selecting an appropriate shape of the jet.

Additionally, some non-traditional methods have been adopted to improve the machining localization and machining accuracy of the Jet-ECM. Rajurkar and Zhu [17] used an eccentric orbital movement of anode workpiece to improve the process stability of the Jet-ECM, thereby reducing the repetition error and improving its machining accuracy. Pajak and his co-workers [18, 19] demonstrated that applying the laser beam coaxially into the electrolyte-jet can improve the machining localization of Jet-ECM and enhance the surface quality of the machined area. Hackert et al. [20] utilized an additional jet of compressed air to remove the electrolyte and electrolytic products from the machining gap of Jet-ECM, which can reduce the stray current surrounding the nozzle, thereby improve its machining localization. After that, Goel and Pandey [21] verified that the addition of compressed air coaxially surrounding the electrolyte-jet is beneficial to further localize the electrolytic current, which reduces the overcut of the machined holes, and consequently improves its machining accuracy. Michell-Smith et al. [22] applied ultrasonic-assisted Jet-ECM to realize the fabrication of high-accurate micro-sized features. Chen et al. [23] developed a process of conductive mask Jet-ECM to reduce the undercutting of the machined micro-dimples by optimizing the distribution of the electric field in the machining gap, which can improve the machining localization of Jet-ECM. Although the machining localization and machining accuracy of Jet-ECM has been improved significantly because of the abovementioned efforts adopted, the modified Jet-ECM processes are less desirable to satisfy the industrial applications owing to the complicated operating conditions or high process cost. Therefore, our group proposed kerosene-submerged Jet-ECM [24, 25], which has been proven as an effective process to considerably improve the machining localization of Jet-ECM in a relatively simple way. However, this process can only show its best capabilities and advantages under appropriate electrochemical machining parameters. In the application of this process, the machining effects of this process will be weakened when the workpiece surface is relatively large or the electrolytic products generated during the machining are quite more, which may cause the electrolyte and electrolytic products to accumulate on the workpiece surface, thereby affecting its mass transfer environment.

Therefore, to further improve its process capability, it is necessary to eliminate the accumulation of electrolyte and electrolytic products on the anode workpiece surface. Therefore, this paper focuses on optimizing the electrochemical machining parameters of the kerosene-submerged Jet-ECM and investigating the influence of the surface effect and shape effect of the workpiece on the machining characteristics of kerosene-submerged Jet-ECM. In the following sections, the machining characteristics including machining localization and machining accuracy of kerosene-submerged Jet-ECM are investigated experimentally and theoretically. The experiments were carried out on the workpiece with different surface and shapes, i.e., large surface flat workpiece, small surface flat workpiece and curved surface workpiece, illustrated in Figure 1.

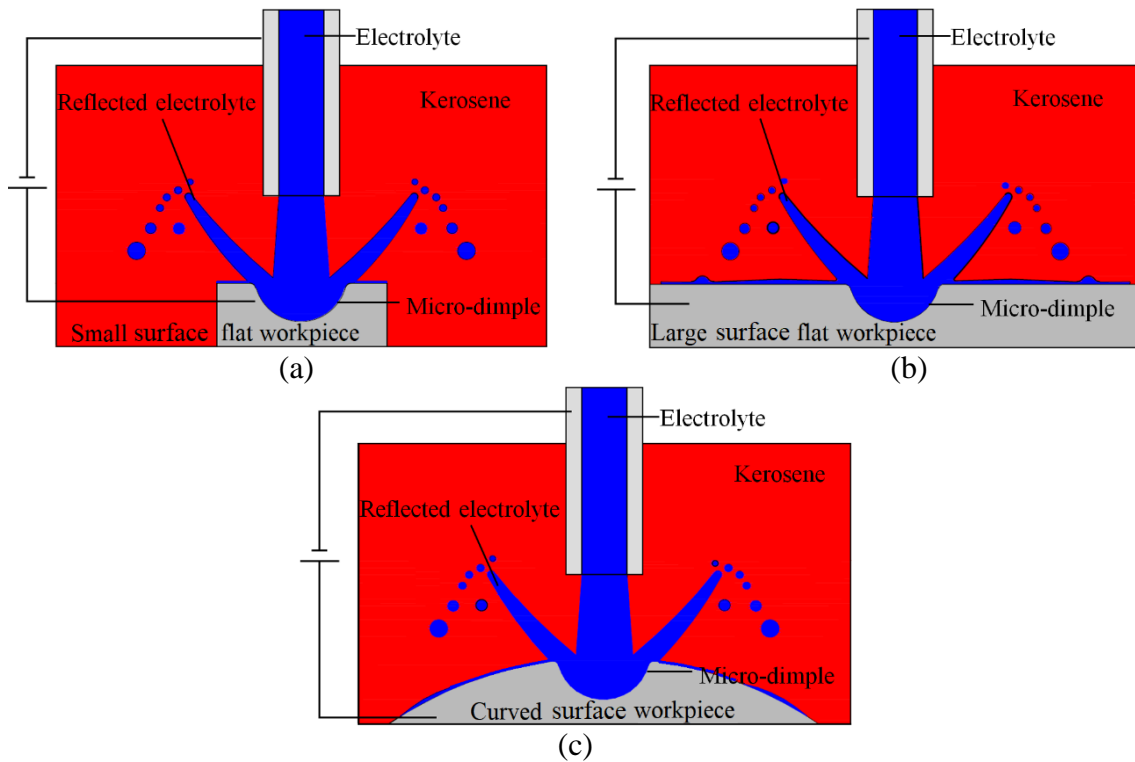


Figure 1. Schematic diagram of the kerosene-submerged Jet-ECM working in the three different cases. (a) Large surface flat workpiece. (b) Small surface flat workpiece. (c) Curved surface workpiece.

2. FLOW FIELD AND ELECTRIC FIELD DISTRIBUTION CHARACTERISTICS OF THE KEROSENE-SUBMERGED Jet-ECM ON THE DIFFERENT WORKPIECE'S SURFACE AND SHAPE

2.1. Physical model

Figure 2 illustrates the schematic diagram of the developed 2D axisymmetric physical models for kerosene-submerged Jet-ECM and traditional Jet-ECM working on different workpiece's surfaces and shapes. Table 1 and Table 2 show the domain definitions and set boundaries conditions of the numerical simulations. Domains I and II denote the electrolyte (its compositions: 20 wt.% NaNO_3 aqueous solution) and the nozzle (its material is SUS 304 stainless steel), respectively. Domain III denotes kerosene/air. Boundary 1 represents the electrolyte inlet. Boundaries 2 and 3 represent the electrolyte outlet. Boundary 4 is anode workpiece surface. Boundary 5 represents the initial interface of the electrolyte. Boundary 6 denotes the symmetry axis. And the other boundaries are wall boundaries.

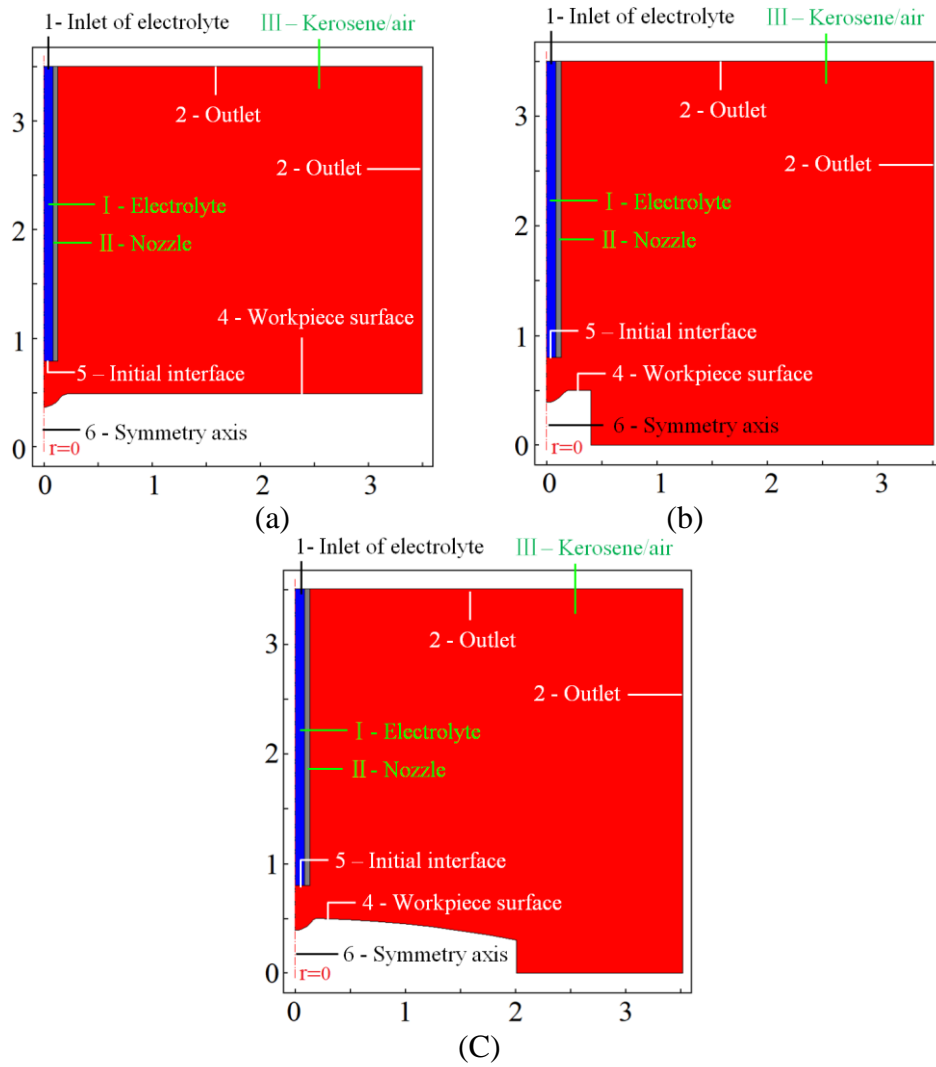


Figure 2. Domain and boundary definitions of the physical models of the kerosene-submerged Jet-ECM and the traditional Jet-ECM working on different workpiece's surface and shapes. (a) Large surface flat workpiece. (b) Small surface flat workpiece. (c) Curved surface workpiece.

Table 1. Domain definitions of the physical models for the kerosene-submerged Jet-ECM and the traditional Jet-ECM.

| Domain definitions | Domain number | Property |
|-----------------------------------|---------------|------------------------------------|
| Fluid property | I | 20 wt.% NaNO ₃ solution |
| Nozzle materials | II | SUS 304 stainless steel |
| Fluid property | III | Kerosene/air |
| Initial values of the electrolyte | I | $U_{init} = 0, P_{init} = 0$ |
| Initial values of the kerosene | III | $U_{init} = 0, P_{init} = 0$ |
| Gravity | I, III | $g_r = 0, g_z = -g$ |

The electrolyte inlet of is assumed to be in the laminar state. Its input pressure of the electrolyte inlet is 1 MPa. The pressure of the electrolyte outlet is maintained to be zero. And the electrolyte conductivity is approximately 15 S/m, which was measured by the conductivity meter.

To simplify the simulation calculation and enhance simulation convergence without loss of generality, some assumptions were made as follow:

- (i) Electrolyte is a continuous incompressible viscous fluid;
- (ii) The electrolyte temperature and conductivity remain constant, and its energy loss is ignored during the machining;
- (iii) Current efficiency is 100%;
- (iv) The mass transfer efficiency is high enough due to the electrolyte-jet flow velocity is very big, therefore, the concentration polarization effect is neglected.

Table 2. Boundary conditions of the physical models of the kerosene-submerged Jet-ECM and the traditional Jet-ECM.

| Boundary conditions | Boundary number | Property |
|---------------------|-----------------|--|
| Electrolyte inlet | 1 | Laminar inflow, $\Phi=0, P_{input} = 1 \text{ MPa}$ |
| Electrolyte outlet | 2, 3 | $P_{outlet} = 0 \text{ MPa}$ |
| Workpiece surface | 4 | No slip ($V = 0$) |
| Initial interface | 5 | |
| Symmetry axis | 6 | |
| Wall | Others | No slip ($V = 0$) |

Since kerosene-submerged Jet-ECM and traditional Jet-ECM involves a typical two-phase fluid phenomenon and the level set method is commonly used to solve the movement and change problems of the double-phase interface or multiple-phase interface [26], it is introduced here to calculate the distribution characteristics of the flow field of kerosene-submerged Jet-ECM and traditional Jet-ECM on different workpiece's surface and shape. The level set function is a continuous function, which utilizes the level set variable Φ to describe the fluid phase type. For the kerosene-submerged Jet-ECM, $0 < \Phi < 0.5$ and $0.5 < \Phi < 1$ represent the electrolyte phase and kerosene phase. And for the traditional Jet-ECM, $0 < \Phi < 0.5$ and $0.5 < \Phi < 1$ represent the electrolyte phase and air phase. Especially, $\Phi=0.5$ is typically regarded as kerosene-electrolyte interface or the air-electrolyte interface. The following equation is applied to characterize the convection of the reinitialized level set function:

$$\frac{\partial \phi}{\partial t} + \nabla \cdot (\phi u) + \gamma \left[\left(\nabla \cdot \left(\phi (1 - \phi) \frac{\nabla \phi}{|\nabla \phi|} \right) \right) - \varepsilon \nabla \cdot \nabla \phi \right] = 0 \quad (1)$$

Here, u represents the flow velocity of kerosene-electrolyte interface or air-electrolyte interface, and γ represents initial flow velocity of kerosene-electrolyte interface or air-electrolyte interface; ε represents the thickness of kerosene-electrolyte interface or air-electrolyte interface.

The secondary current distribution theory was employed to calculate the distribution of electric field of the model due to the concentration polarization is neglected.

2.2. Governing equations and boundary conditions

The Navier-Stokes equation is applied to describe the transport of mass and momentum of the electrolyte, kerosene, air and the kerosene-electrolyte interface or air-electrolyte interface, which is expressed as follow:

$$\rho \left(\frac{\partial u}{\partial t} + u \cdot \nabla u \right) - \nabla \cdot (\mu (\nabla u + \nabla u^T)) + \nabla p = F_{st} \quad (2)$$

$$(\nabla \cdot u) = 0 \quad (3)$$

Here, p represents the pressure, F_{st} represents surface tension, which is calculated by formula (4).

$$F_{st} = \nabla \cdot T \quad (4)$$

$$T = \sigma (I - (nn^T)) \delta \quad (5)$$

Here, I denotes the unit matrix; n denotes interface normal, which can be calculated by formulas (6); σ denotes the surface tension coefficient (N/m); δ denotes delta function. It is not equal to zero only at their interface, which can be calculated approximately by the formulas (7).

$$n = \frac{\nabla \phi}{|\nabla \phi|} \quad (6)$$

$$\delta = 6 |\phi(1-\phi)| |\nabla \phi| \quad (7)$$

Butler-Volmer equation, shown as formula (8), is selected to calculate the electric field distribution, because the electrochemical reactions are completely dominated by activation controlled current.

$$i = i_0 \left(\exp\left(\frac{\alpha_a F \eta}{RT}\right) - \exp\left(\frac{\alpha_c F \eta}{RT}\right) \right) \quad (8)$$

$$\eta = E - E_{eq} \quad (9)$$

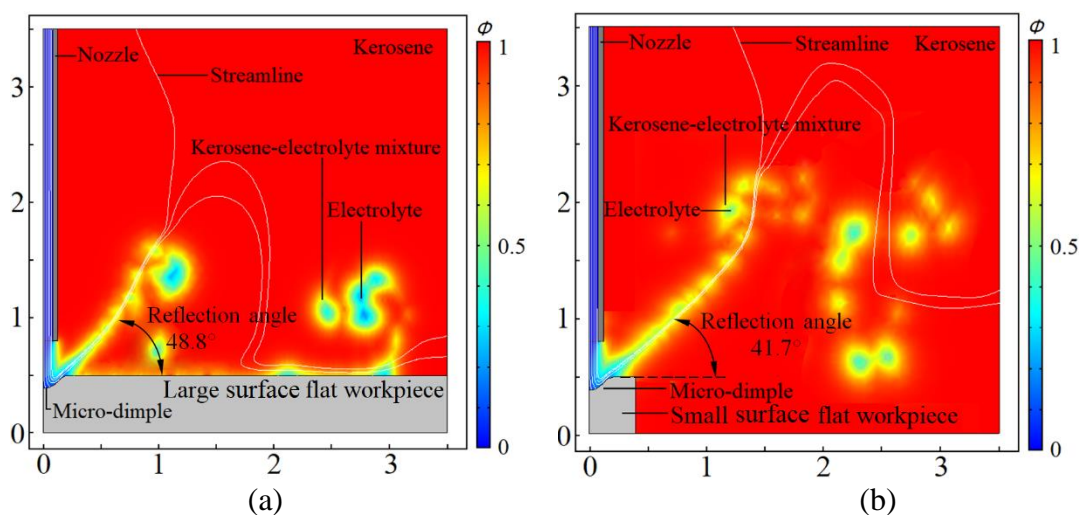
Here, i denotes current density; i_0 denotes exchange current density; η denotes overpotential; F denotes Faraday constant (96485 C/mol); α_a denotes anodic transfer coefficient; α_c denotes cathodic transfer coefficient; T denotes Kelvin Temperature; E denotes electrode potential; E_{eq} denotes equilibrium potential.

The software of COMSOL Multiphysics (5.3 versions) is applied to calculate the coupled flow field and electric field distribution characteristics of kerosene-submerged Jet-ECM and traditional Jet-ECM on the workpieces with different surface and shapes.

2.3. Simulation results and discussion

Figure 3 shows the distribution characteristics of the flow field of kerosene-submerged Jet-ECM working in three different cases. For comparative analysis, the flow field distribution characteristics of traditional Jet-ECM working in three different cases are also studied, shown in Figure 4. It was found that the reflection phenomenon of the electrolyte can be observed in both the kerosene-submerged Jet-ECM and the traditional Jet-ECM, but its reflection behaviors are much different depending on the medium surrounding the impinging electrolyte-jet, which is similar to the reflection phenomenon of the

electrolyte simulated in our published paper [24]. When the surrounding medium is kerosene, the reflected electrolyte almost does not touch the outside wall of the nozzle regardless of the workpiece's surface and shape. However, when the surrounding medium is air, the reflected electrolyte continuously touches the outside wall of the nozzle, which can lead to a secondary electric contact phenomenon at the edge of the micro-dimples. This result was also reported by Hackert et al. [13]. These differences reveal that, in the kerosene-submerged Jet-ECM, the occurrence of reflected electrolyte contacting the nozzle outside wall almost disappears, which is beneficial to reduce the secondary electric contact corrosion in the non-machined area. It was also discovered that, in the same surrounding medium, the reflection behaviors vary with the workpiece's surface and shape. In the kerosene-submerged environment, the reflection angle gets smaller, from 48.8° to 41.7° , when the area of the workpiece surface impinged by the electrolyte-jet decreases, and it reduces to be the minimal (36.9°) when the electrolyte-jet impinges on the curved surface workpiece. In traditional Jet-ECM with an air ambient environment, a similar trend can be found, but the corresponding value of the reflection angle is slightly larger than the reflection angle in kerosene-submerged Jet-ECM. Besides, the phenomenon of the hydraulic jump disappears when electrolyte-jet impinges on the small surface flat workpiece and curved surface workpiece. The main reasons for these differences are: (i) The specific gravity of the kerosene is significantly larger than the air, which indicates that the kerosene has a much bigger impedance to the movement of the reflected electrolyte than the air. Therefore, the presence of the kerosene leads to a weaker reflection of the electrolyte in the kerosene-submerged case, which can reduce the secondary electric contact corrosion in the non-machined area of Jet-ECM; (ii) The efficient discharge of the impinged electrolyte-jet on the surface of the small surface flat workpiece and curved surface workpiece make the accumulation of the electrolyte on the workpiece surface disappear. These findings indicate that the kerosene-submerged environment can significantly reduce the possibility of the reflected electrolyte contacting with the outside wall of the cathode nozzle, thereby reducing the secondary electric current corrosion significantly. And the small surface flat workpiece and curved surface workpiece can promote the discharge of electrolyte and electrolytic products, which can create better mass transfer conditions for Jet-ECM.



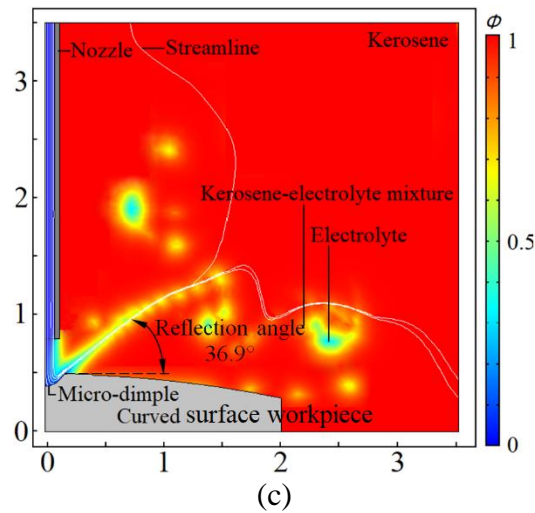


Figure 3. The distribution of flow field of kerosene-submerged Jet-ECM on the different workpiece's surface and shape. (a) Large surface flat workpiece. (b) Small surface flat workpiece. (c) Curved surface workpiece.

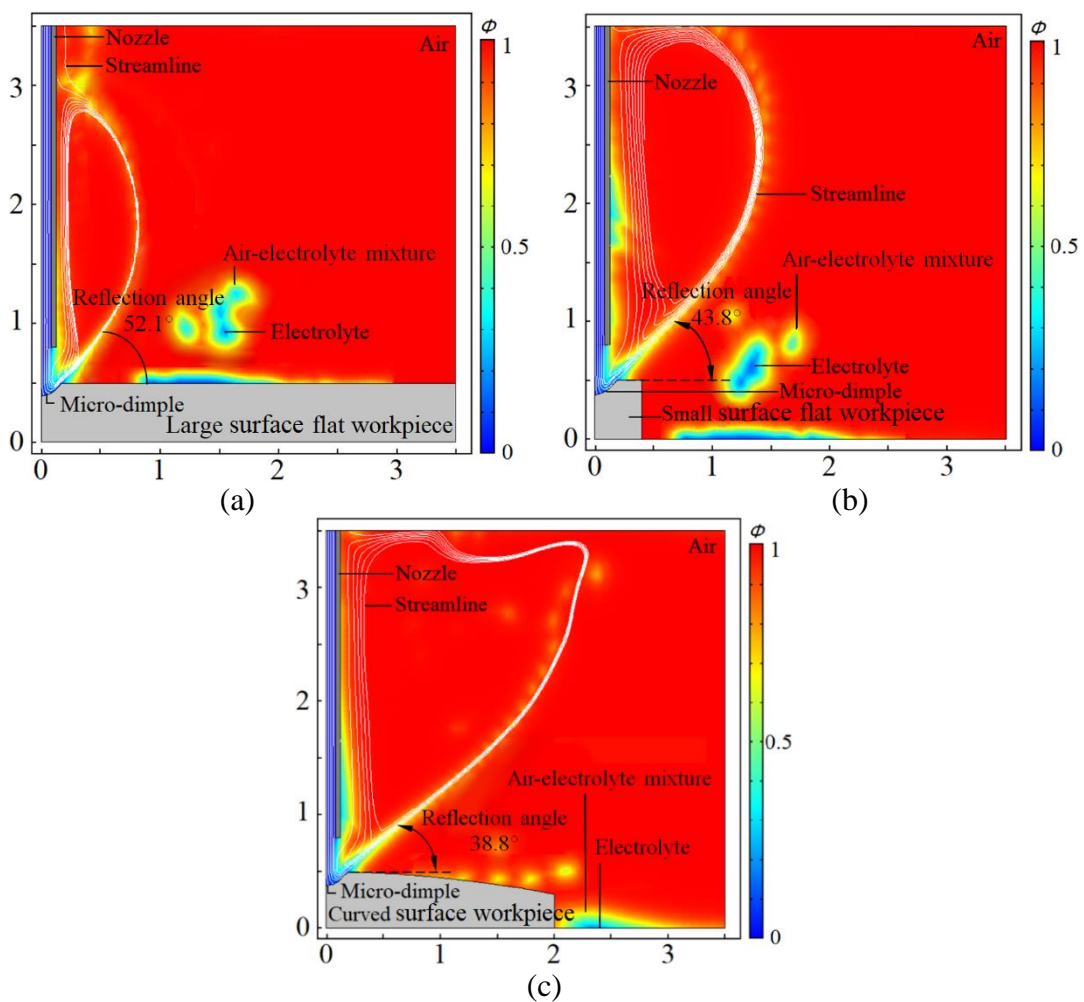


Figure 4. The distribution of flow field of traditional Jet-ECM on different workpiece's surface and shape. (a) Large surface flat workpiece. (b) Small surface flat workpiece. (c) Curved surface workpiece.

Figure 5 and Figure 6 respectively show the distribution characteristics of the electric field of kerosene-submerged Jet-ECM and traditional Jet-ECM on the different workpiece's surface and shape. Generally, there is a significant difference in the electric field distribution between the kerosene-submerged case and the air-submerged case on the same type of workpiece. It is found that compared with traditional Jet-ECM, the electric field distribution of kerosene-submerged Jet-ECM is more concentrated on the same type of workpiece due to the presence of kerosene medium. Besides, an evident variation takes place with the change of workpiece's surface and shape. The electric field distribution is more localized when the small surface flat workpiece and the curved surface workpiece are machined, which is closely relevant to the flow field distribution characteristics of the electrolyte-jet impinged on the workpiece surface. The electrolyte film on the small surface flat workpiece and curved surface workpiece is much thinner due to the electrolyte can be effectively removed from the small surface flat workpiece and the curved surface workpiece, which can increase the electrical resistance of the electrolyte film, and thus reducing the stray current of the non-machining area on the small surface flat workpiece and the curved surface workpiece. These findings can be further verified by the current density distribution on the anode workpiece surface, shown in Figure 7. The results show that compared with traditional Jet-ECM, an improved machining localization is able to be obtained in kerosene-submerged case. Besides, a considerably reduced stray current is detected in kerosene-submerged Jet-ECM. Additionally, compared with the large surface flat workpiece, Jet-ECM working on the small surface flat workpiece and curved surface workpiece enables to obtain a more localized current density distribution and a reduced stray current.

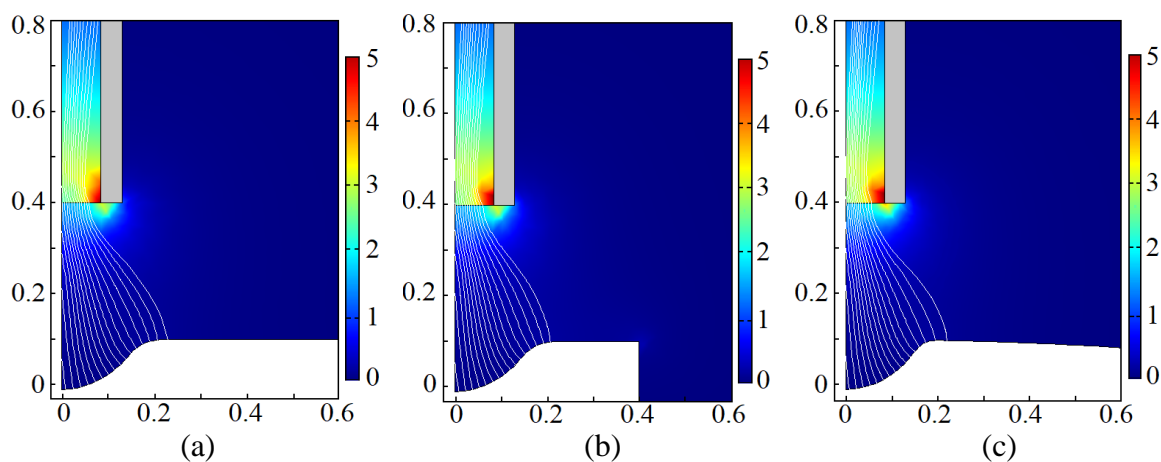


Figure 5. The electric field distribution of kerosene-submerged Jet-ECM on the different workpiece's surface and shape. (a) Large surface flat workpiece. (b) Small surface flat workpiece. (c) Curved surface workpiece.

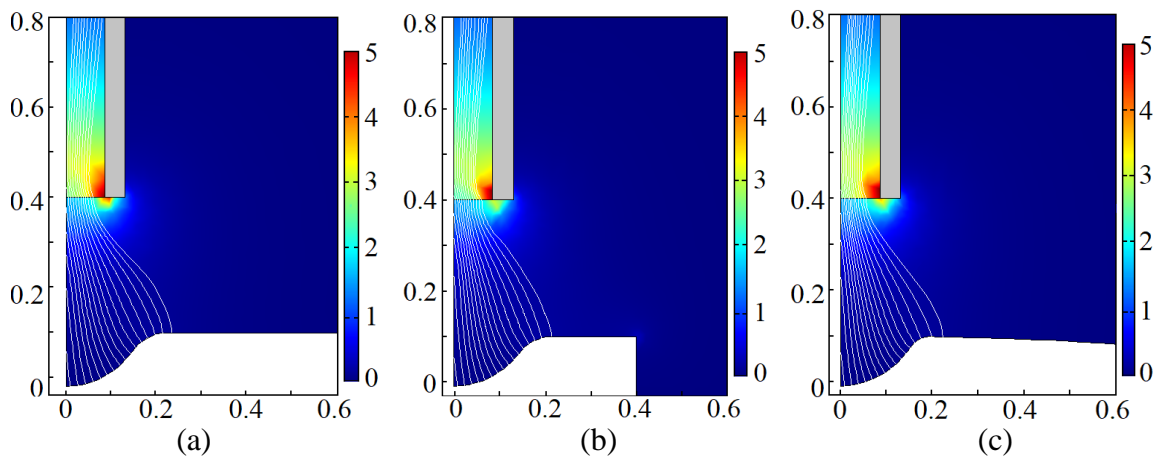


Figure 6. The electric field distribution of traditional Jet-ECM on different workpiece's surface and shape. (a) Large surface flat workpiece. (b) Small surface flat workpiece. (c) Curved surface workpiece.

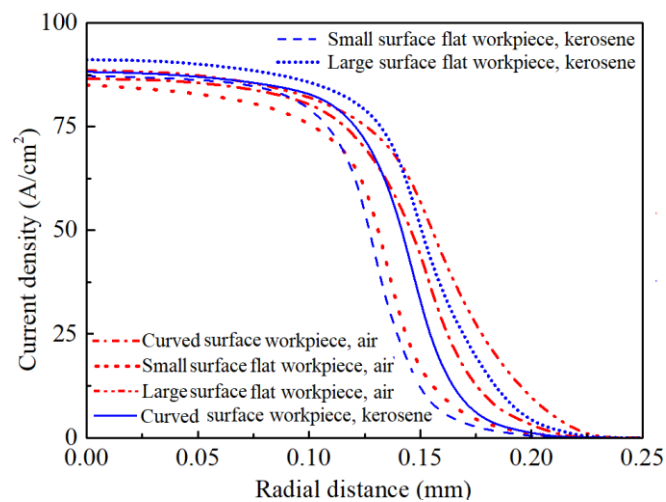


Figure 7. The distribution of current density on the anodic workpiece surface of kerosene-submerged Jet-ECM and traditional Jet-ECM on the different workpiece's surface and shape.

In conclusion, the results show that the surface effect and shape effect of the workpiece and the type of the medium surrounding the electrolyte-jet have a great effect on the flow field distribution and electric field distribution of the Jet-ECM, and thus have a great influence on its machining localization and the resultant of the geometric profiles, machining accuracy and surface quality of the machined microstructures.

3. EXPERIMENTAL

To assess the real effect of the workpiece's surface and shape on the machining characteristics of the kerosene-submerged Jet-ECM, experiments were carried out to fabricate micro-dimples as examples. The used setup had been described in detail in our published paper [24]. And 20wt.%

sodium nitrate (NaNO_3) solution was applied. The input pressure of the electrolyte inlet was 1 MPa. The electrolyte temperature and kerosene temperature were 25 °C. The inner diameter of the nozzle (its material is SUS304 stainless steel) was 170 μm . The machining gap between the anode workpiece surface and the cathode nozzle was 300 μm . SUS304 stainless steel plates with a diameter of 40 mm and a diameter of 0.8 mm (its thickness about 1 mm) were used as the large surface flat workpiece and small surface flat workpiece, respectively. And the outside wall of a SUS304 stainless steel pipe with a diameter of 48 mm was used as the curved surface workpiece. The machining voltage was 10 V-25 V with an increment of 5 V during machining. The machining time of the fabricated micro-dimple was 15 s. The main experimental conditions and parameters were presented in Table 3.

Table 3. The main experimental conditions and parameters for experimentation.

| Machining parameter | Property or value |
|--|--------------------------|
| Nozzle material | SUS 304 stainless steel |
| Nozzle diameter, μm | 170 |
| Electrolyte | NaNO_3 solution |
| Concentration, wt. % | 20 |
| Electrolyte conductivity, S/m | 15 |
| Workpiece material | SUS 304 stainless steel |
| The input pressure of the electrolyte-jet, MPa | 1 |
| Machining gap, μm | 300 |
| Machining voltage, V | 10-25 |
| Electrolyte outlet pressure, MPa | $P = 0$ |
| Machining time, s | 15 |
| Temperature of the electrolyte, °C | 25 |
| Temperature of the kerosene, °C | 25 |

The scanning electron microscope (Merlin Compact, Carl Zeiss NTS GmbH Corp., Oberkochen, Germany) and the digital microscope (VHX-2000, Keyence Corp., Osaka, Japan) were applied to characterize the machined micro-dimples.

Generally, overcut is inevitable during ECM due to the isotropic dissolution behavior of the metallic workpiece material. The etch factor (EF), representing the ratio of material removal depth, h , to the overcut length, $(d-d_0)/2$, of the machined micro-dimple in the through-mask electrochemical machining [27], was introduced to assess the machining localization of Jet-ECM quantitatively, which is defined by the formula (10).

$$EF = 2h/(d - d_0) \quad (10)$$

Here, h denotes the micro-dimple's depth, d denotes the micro-dimple's diameter, and d_0 represents nozzle's inner diameter used in the experiment. A larger etch factor (EF) means a higher machining localization.

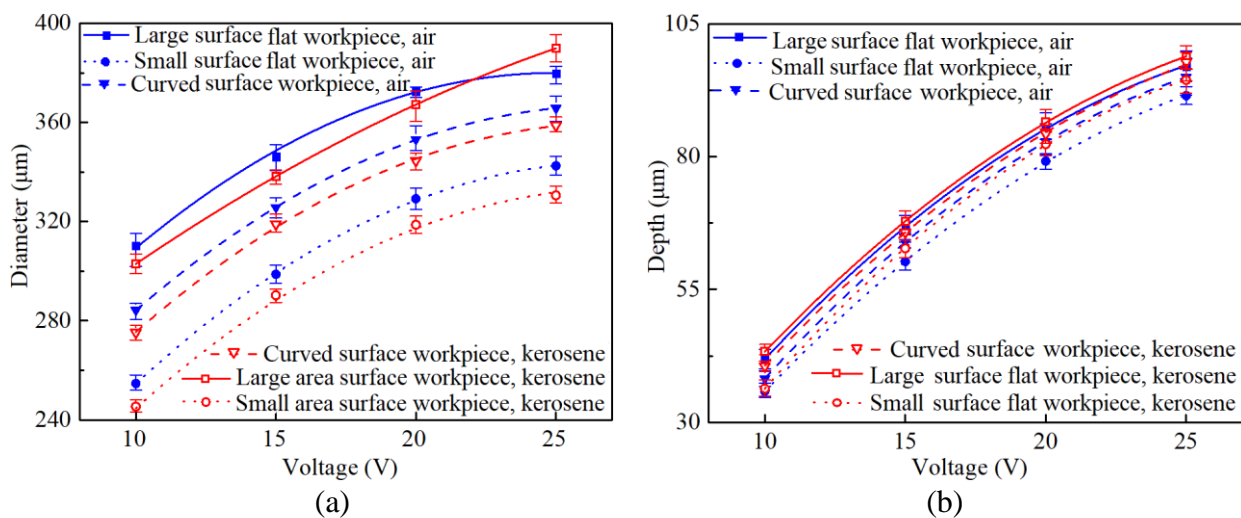
Additionally, the standard deviation of the diameter and depth of the machined micro-dimples

is introduced to assess the machining accuracy. The smaller the standard deviation of the diameter and the depth of the micro-dimples is, the better the geometric dimensional consistency and machining accuracy of the machined features are.

4. RESULTS AND DISCUSSION

4.1. Geometric dimensional of the machined micro-dimples

Figure 8 shows the change trends of the diameter, depth and, etch factor (EF) of the micro-dimples machined by kerosene-submerged Jet-ECM and traditional Jet-ECM on different workpiece's surface and shape with a varying machining voltage. It can be found that whether in kerosene-submerged Jet-ECM or traditional Jet-ECM, the diameter, depth and EF of the fabricated micro-dimples increase with increasing machining voltage, but their respective increment gradually decreases, which has the the same growth trend with the micro-dimple fabricated by Zhang et al. [10]. And their change trend is highly dependent on the workpiece's surface and shape used. Smaller micro-dimples with bigger EF can be achieved when the electrolyte-jet impinges on the small surface flat workpiece and curved surface workpiece, while when the electrolyte-jet is working on the large surface flat workpiece, larger micro-dimples with smaller EF can be fabricated. This is due to the electrolyte and electrolytic products can be discharged smoothly on the small surface flat workpiece and curved surface workpiece, and thus leading to a better mass transfer environment and machining conditions. This fact of the smooth discharge of electrolyte and electrolytic products from the machining gap can improve the machining localization and machining accuracy of Jet-ECM has also been demonstrated by Thanigaivelan et al. [9] and Hackert et al. [20]. These experimental findings verified that the machining localization of kerosene-submerged Jet-ECM is considerably relevant to the workpiece's surface and shape. Further, the influence of the workpiece's surface and shape on the diameter, depth, and EF (or machining localization) of the micro-dimples was also certificated in traditional Jet-ECM.



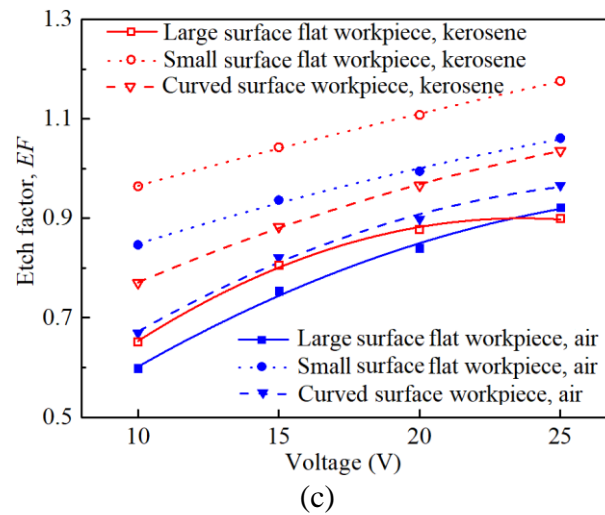


Figure 8. The variation of geometric dimensions of the micro-dimples produced on different workpiece's surface and shape with different machining voltage in kerosene-submerged Jet-ECM and traditional Jet-ECM when the machining gap is 0.3 mm and machining time is 15 s. (a) Diameter. (b) Depth. (c) Etch factor, EF .

In addition, it was found that the geometric dimensions of the machined micro-dimples are closely related to the medium surrounding the impinging electrolyte-jet. Compared with the air medium, the smaller and deeper micro-dimples can be achieved when the electrolyte-jet impinges on the small surface flat workpiece and curved surface workpiece in the kerosene medium, which means a bigger EF value can be achieved. Therefore, an improved machining localization can be achieved on the small surface flat workpiece and curved surface workpiece in kerosene-submerged Jet-ECM than traditional Jet-ECM. However, some differences existed on the large surface flat workpiece. When the electrolyte-jet impinges on the large surface flat workpiece in the kerosene medium, smaller and deeper micro-dimples can be obtained only at the low machining voltage than the air medium, which implies that a bigger EF value is achieved at the low machining voltage on the large surface flat workpiece in the kerosene medium. This has similar characteristics to the micro-dimples fabricated on the small surface flat workpiece and curved surface workpiece, which implies an improved machining localization can also be achieved on the large surface flat workpiece with the low machining voltage in kerosene-submerged Jet-ECM than in the traditional Jet-ECM. While at large machining voltage, the case is on the contrary. This is related to the workpiece's surface and shape and the medium surrounding the electrolyte-jet. Since kerosene has a much bigger impedance to the movement of the reflected electrolyte, leading to a weaker reflection of the electrolyte in the kerosene-submerged case. On the small surface flat workpiece and curved surface workpiece or on the large surface flat workpiece with low machining voltage, the inhibition effect of kerosene on the stray current plays a major role in reducing stray corrosion. However, more electrolytic products will be generated on the large surface flat workpiece with large machining voltage and it is difficult to be discharged smoothly from the large surface flat workpiece and will accumulate on the large surface flat workpiece. At this time, the impedance effect of kerosene on the discharge of electrolytic products from the workpiece surface begin to dominate, which usually affects its distribution of flow field and electric field, and

thus leading to a large overcut and reducing its machining localization. This indicates that the kerosene-submerged Jet-ECM is able to achieve higher machining localization under better mass transfer environment and electric field conditions.

Figure 9 illustrates the variation trends of the standard deviation of diameter and depth of the micro-dimples machined on different workpiece's surface and shape by kerosene-submerged Jet-ECM and traditional Jet-ECM with different machining voltage. It was found that the standard deviation of the diameter and depth of the micro-dimples depends on the workpiece's surface and shape. Whether in kerosene-submerged Jet-ECM or traditional Jet-ECM, a smaller standard deviation of diameter and depth of the micro-dimples can be obtained when the electrolyte-jet impinges on the small surface flat workpiece and curved surface workpiece, which means the micro-dimples machined on the small surface flat workpiece and curved surface workpiece feature better machining accuracy and higher geometric shape consistency and reproducibility than that fabricated on the large surface flat workpiece.

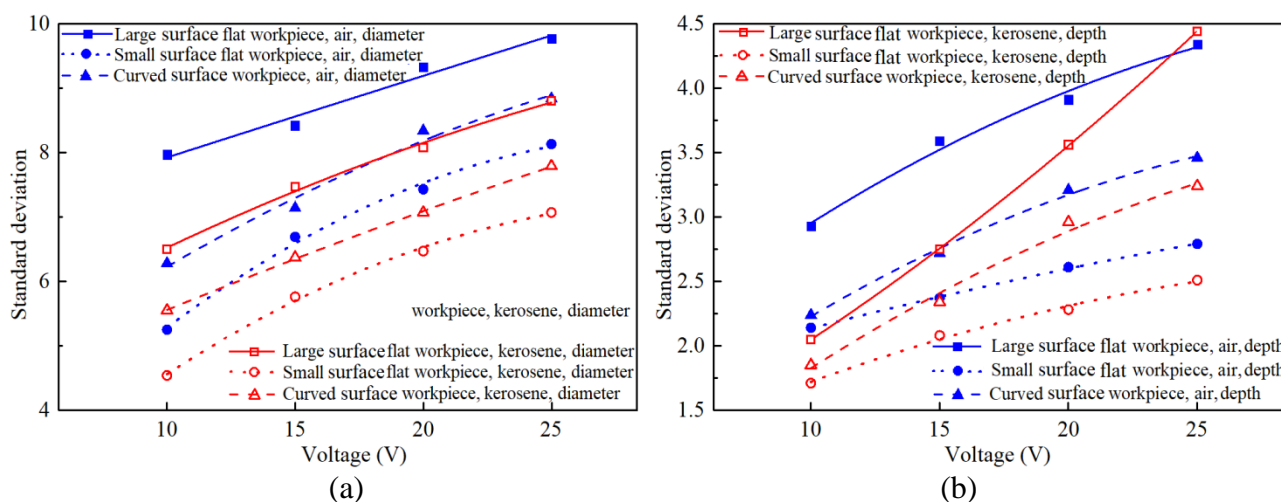


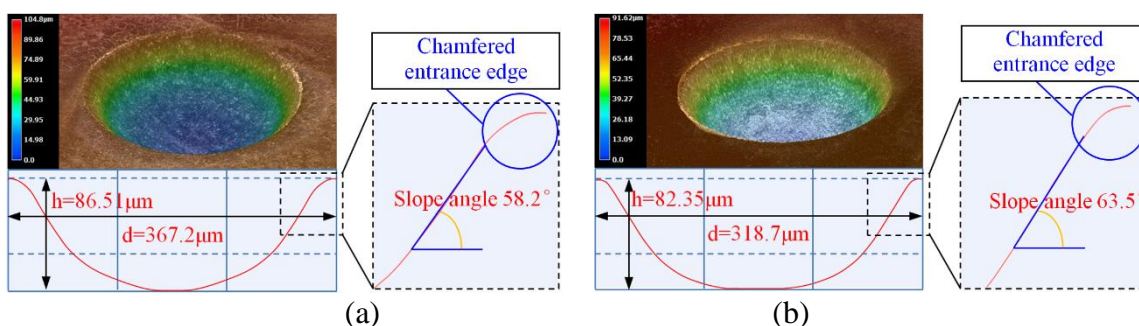
Figure 9. The variation trends of the standard deviation of diameter and depth of the micro-dimples machined on the different workpiece's surface and shape by kerosene-submerged Jet-ECM and traditional Jet-ECM with different machining voltage when the machining gap is 0.3 mm and machining time is 15 s. (a) The standard deviation of the diameter. (b) The standard deviation of the depth.

Besides, it was found that the standard deviation of the diameter and depth of the micro-dimples is associated with the medium surrounding the electrolyte-jet. Compared with the air medium, the standard deviation of diameter and depth of the micro-dimples machined on the small surface flat workpiece and curved surface workpiece in the kerosene medium is smaller regardless of the machining voltage. And at small machining voltage, the standard deviation of diameter and depth of the micro-dimples machined on the large surface flat workpiece by the kerosene-submerged Jet-ECM is also smaller than those fabricated in the traditional Jet-ECM. However, only at big machining

voltage, the standard deviation of diameter and depth of the micro-dimples machined on the large surface flat workpiece by the kerosene-submerged Jet-ECM is larger than those fabricated in the traditional Jet-ECM. This is due to the collective effect of the workpiece's surface and shape and the medium surrounding the electrolyte-jet. Therefore, this demonstrates that the machining accuracy of the micro-dimples machined by kerosene-submerged Jet-ECM on the small surface flat workpiece and curved surface workpiece or on the large surface flat workpiece with small machining voltage is higher than the traditional Jet-ECM.

4.2. Surface morphologies of the fabricated micro-dimples

Figure 10 displays the 3D geometric profiles and morphologies of the machined micro-dimples by kerosene-submerged Jet-ECM on the large surface flat workpiece, small surface flat workpiece and curved surface workpiece, when the machining voltage is 20 V. It can be found that the micro-dimples machined on the large surface flat workpiece by the kerosene-submerged Jet-ECM features a large chamfered entrance edge and a small slope angle of approximately 58.2° . While the micro-dimples fabricated on the small surface flat workpiece and curved surface workpiece feature a smaller chamfered entrance edge and a larger slope angle (for the former, the slope angle: 63.5° ; for the latter, the slope angle: 60.8°). This result demonstrates that compared with the micro-dimples machined on the large surface flat workpiece, the micro-dimples machined on the small surface flat workpiece and curved surface workpiece yields a smaller overcut and a higher machining localization. This phenomenon further proves that the machining localization of the kerosene-submerged Jet-ECM is closely related to the workpiece's surface and shape. And the influence of the workpiece's surface and shape on the machining localization of the Jet-ECM can also be further demonstrated by the 3D geometric profiles and morphologies of the fabricated micro-dimples by the traditional Jet-ECM, shown in Figure 11. In traditional Jet-ECM, a similar trend of the slope angle can also be found, but the micro-dimples machined by traditional Jet-ECM displays a rounded entrance edge with a reduced slope angle when the micro-dimples machined on the same type of workpiece. This similar rounded edge phenomenon on the entrance of the micro-dimple is in a good agreement with the report of Hackert et al. [28]. This demonstrates that there is more stray corrosion at the entrance edge of the micro-dimples fabricated by traditional Jet-ECM. Therefore, this phenomenon proves that compared with traditional Jet-ECM, kerosene-submerged Jet-ECM can yield the micro-dimples with a smaller overcut and achieve higher machining localization.



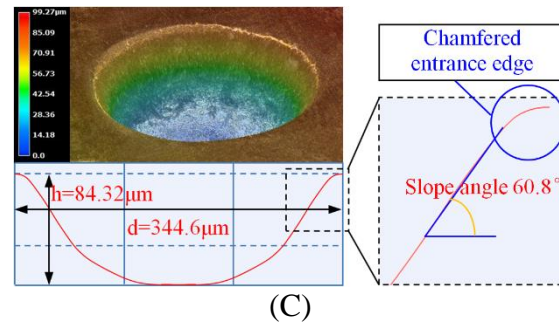


Figure 10. Geometric profiles and morphologies of the machined micro-dimples by kerosene-submerged Jet-ECM on different workpiece's surface and shape with machining gap of 0.3 mm and machining time of 15 s when the machining voltage is 20 V. (a) Large surface flat workpiece. (b) Small surface flat workpiece. (c) Curved surface workpiece.

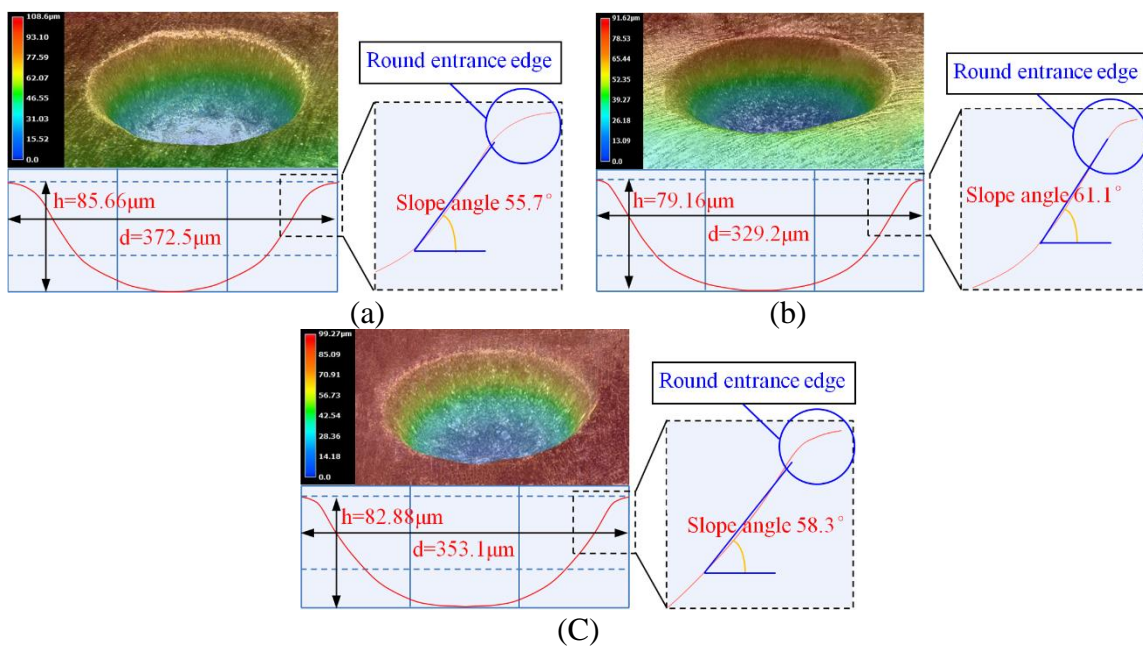


Figure 11. Geometric profiles and morphologies of the machined micro-dimples by traditional Jet-ECM on different workpiece's surface and shape with machining gap of 0.3 mm and machining time of 15 s when the machining voltage is 20 V. (a) Large surface flat workpiece. (b) Small surface flat workpiece. (c) Curved surface workpiece.

Figure 12 illustrates the SEM images of the micro-dimples machined by kerosene-submerged Jet-ECM on the workpiece with different surfaces and shapes when the machining voltage is 20 V. It can be found that kerosene-submerged Jet-ECM can produce smoother surface on the small surface flat workpiece and curved surface workpiece than large surface flat workpiece. Besides, there is no obvious stray corrosion at the entrance of the fabricated micro-dimples and the non-machining areas surrounding the fabricated micro-dimple on the small surface flat workpiece and the curved surface workpiece, but the obvious stray corrosion phenomenon can be observed on a large surface flat workpiece. This phenomenon indicates that kerosene-submerged Jet-ECM working on the small surface flat workpiece and curved surface workpiece can fabricate micro-dimples with better surface

quality. This result related to the workpiece's surface and shape can also be further proved by the SEM images of the micro-dimples machined by traditional Jet-ECM on the workpiece with different surfaces and shapes, shown in Figure 13. Further, compared with the kerosene-submerged Jet-ECM, micro-dimples machined by the traditional Jet-ECM are coarser. Besides, more obvious stray corrosion can be observed at the entrance of the micro-dimples and the non-machining areas surrounding the micro-dimples machined in the traditional Jet-ECM when the micro-dimples fabricated on the same type of workpiece, which indicates that micro-dimples with better surface quality can be fabricate in the kerosene-submerged case.

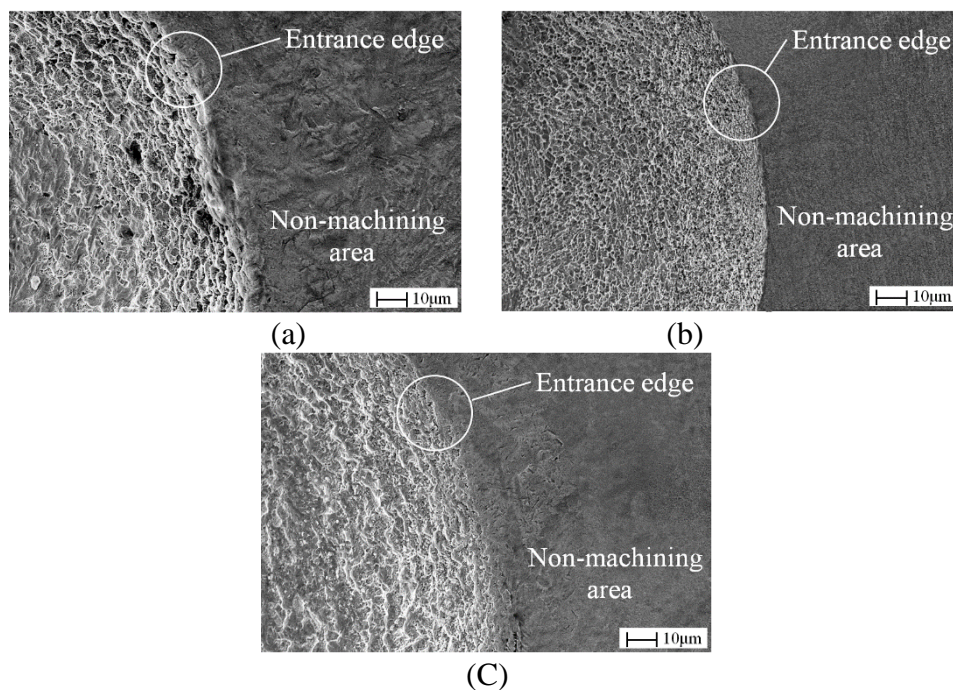
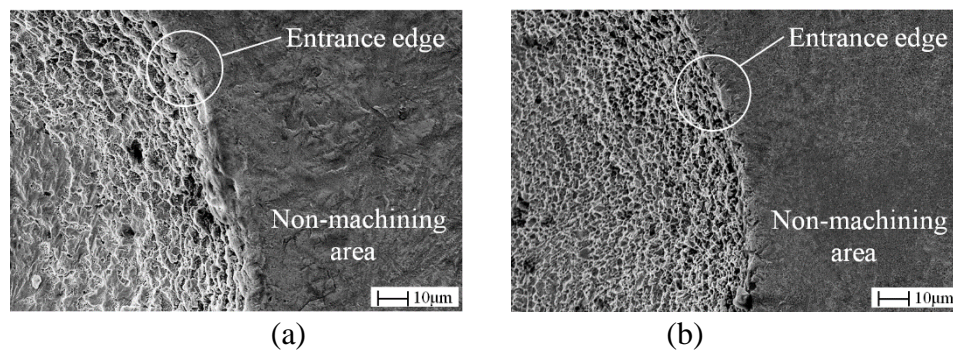


Figure 12. SEM images of the fabricated micro-dimples by kerosene-submerged Jet-ECM on different workpiece's surface and shape with machining gap of 0.3 mm and machining time of 15 s when the machining voltage is 20 V. (a) Large surface flat workpiece. (b) Small surface flat workpiece. (c) Curved surface workpiece.



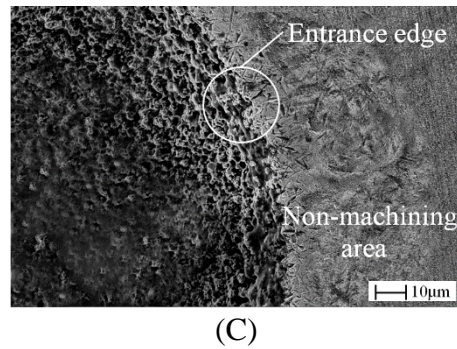


Figure 13. SEM images of the machined micro-dimples by the traditional Jet-ECM on different workpiece's surface and shape with machining gap of 0.3 mm and machining time of 15 s when the machining voltage is 20 V. (a) Large surface flat workpiece. (b) Small surface flat workpiece. (c) Curved surface workpiece.

In summary, the workpiece's surface and shape and the type of the medium surrounding the electrolyte-jet have a great effect on the machining localization and machining accuracy of Jet-ECM. Kerosene medium instead of the air medium surrounding the electrolyte-jet can improve the machining localization of Jet-ECM and enhance the machining accuracy and surface quality of the machined microstructures. And kerosene-submerged Jet-ECM working on the small surface flat workpiece and curved surface workpiece can achieve higher machining localization. Besides, high accuracy microstructure with smooth surface can be fabricated by Jet-ECM on the small surface flat workpiece and curved surface workpiece.

5. CONCLUSIONS

Although kerosene-submerged Jet-ECM has been proven as an effective process to enhance the machining localization of the Jet-ECM, the process can only show its best capabilities and advantages under appropriate electrochemical machining parameters. In the application of this process, its machining effects will be weakened when the workpiece surface is relatively large or the electrolytic products generated during the machining are quite more, which may cause the electrolyte and electrolytic products to accumulate on the workpiece surface, thereby affecting its mass transfer environment. Therefore, to further improve its process capability, it is necessary to eliminate the accumulation of electrolyte and electrolytic products on the workpiece. And thus, this paper focuses on optimizing the electrochemical machining parameters of the kerosene-submerged Jet-ECM and investigating the surface effect and shape effect of the workpiece on the machining localization and machining accuracy experimentally and theoretically. Numerical simulations were carried out to understand the machining characteristics and mechanisms of kerosene-submerged Jet-ECM on different workpiece's surface and shape. The conclusions are as follows:

(1) The surface effect and shape effect of the workpiece and the type of the medium surrounding the electrolyte-jet have a significant influence on the machining localization of Jet-ECM. Kerosene medium instead of the air medium surrounding the electrolyte-jet can improve the machining localization of Jet-ECM. And kerosene-submerged Jet-ECM working on the small surface flat

workpiece and curved surface workpiece can achieve higher machining localization than the large surface flat workpiece.

(2) In the kerosene-submerged Jet-ECM, high accuracy microstructure with better surface quality can be fabricated due to kerosene medium has a much bigger impedance to the movement of the reflected electrolyte, which can prevent the reflected electrolyte from contacting the outer wall of the nozzle, and thus reducing the stray electric field around the nozzle.

(3) The implementation of the kerosene-submerged Jet-ECM on the small surface flat workpiece and curved surface workpiece is able to fabricate micro-sized features with higher machining accuracy and better surface quality than on the large surface flat workpiece since the electrolyte and electrolytic products can be discharged smoothly on the small surface flat workpiece and curved surface workpiece, and thus leading to a better mass transfer environment and machining conditions.

ACKNOWLEDGEMENT

This work was financially supported by the NSFC of China [No. 51875178], Key scientific and technological projects of Henan Province [No. 202102210069] and Key Scientific Research Project of Colleges and Universities in Henan Province [No. 19A460022].

References

1. M. M. Lohrengel, K. P. Rataj, N. Schubert, M. Schneider, S. Höhn, A. Michaelis, M. Hackert-Oschätzchen, A. Martin and A. Schubert, *Powder Metall.*, 57 (2014) 21.
2. M. Hackert-Oschätzchen, G. Meichsner, M. Zinecker, A. Martin and A. Schubert, *Precis. Eng.*, 36 (2012) 612.
3. A. Martin, C. Eckart, N. Lehnert, M. Hackert-Oschätzchen and A. Schubert, *Procedia Cirp*, 45 (2016) 231.
4. W. Natsu, S. Ooshiro and M. Kunieda, *Cirp Journal of Manufacturing Science and Technology*, 1 (2018) 27.
5. T. Kawanaka, S. Kato, M. Kunieda, J. W. Murray and A. T. Clare, *Procedia CIRP*, 13 (2014) 345.
6. M. Sen and H. S. Shan, *Int J. Adv. Manuf. Tech.*, 31 (2006) 520.
7. Y. Q. Yu, J. S. Zhao, B. H. Li and J. W. Xu, *Key Eng. Mater.*, 458 (2010) 307.
8. J. Mitchell-smith, A. Speidel and A. T. Clare, *J. Manuf. Process.*, 31 (2018) 273.
9. R. Thanigavelan, R. M. Arunachalam, B. Karthikeyan and P. Loganathan, *Procedia CIRP*, (2013) 351.
10. X. M. Zhang, X. D. Song, P. M. Ming, X. C. Li, Y. B. Zeng, J. T. Cai. *Micromachines*, 10 (2019), 404.
11. J. Kozak, K. P. Rajurkar and R. Balkrishna, *Journal of Manufacturing Science and Engineering*, Trans. ASME, 118 (1996) 490.
12. M. Hackert-Oschätzchen, R. Paul, M. Kowalick, A. Martin, G. Meichsner and A. Schubert, *Procedia CIRP*, 31 (2015) 197.
13. M. Hackert-Oschätzchen, R. Paul, A. Martin, G. Meichsner, N. Lehnert and A. Schubert, *J. Mater. Process. Technol.*, 223 (2015) 240.
14. J. Mitchell-smith, A. Speidel, J. Gaskell and A.T. Clare, *Int. J. Mach. Tools Manuf.*, 122 (2017) 32.
15. J. Mitchell-smith, A. Speidel and A.T. Clare, *J. Mater. Process. Technol.*, 255 (2018) 364.

16. X. D. Wang, N. S. Qu and X. L. Fang, *J. Mater. Process. Technol.*, 264 (2019) 240.
17. K. P. Rajurkar and D. Zhu, *CIRP Ann-Manuf. Technol.*, 48 (1999) 139.
18. A. K. M. Desilva, P. T. Pajak, D. K. Harrison and J. A. McGeough, *CIRP Annals*, 53 (2004) 179.
19. P. T. Pajak, A. K. M. Desilva, D. K. Harrison and J. A. McGeough, *Precis. Eng.-J. Int. Soc. Precis. Eng. Nanotechnol.*, 30 (2006) 288.
20. M. Hackert-Oschätzchen, G. Meichsner, A. Schubert, *European Society for Precision Engineering and Nanotechnology, EUSPEN*, 2 (2008) 420.
21. H. Goel and P. M. Pandey, *Proc. Inst. Mech. Eng. Part B-J. Eng. Manuf.*, 232 (2016) 451.
22. J. Mitchell-Smith and A.T. Clare, *Procedia CIRP*, 42 (2016) 379.
23. X. L. Chen, B. Y. Dong, C.Y. Zhang, M. Wu and Z. N. Guo, *J. Mater. Process. Technol.*, 257 (2018) 101.
24. P. M. Ming, X. C. Li, X. M. Zhang, X. D. Song, J. T. Cai, G. Qin, L. Yan and X. S. Zheng, *Procedia CIRP*, 68 (2018) 432.
25. X. C. Li, P. M. Ming, X. M. Zhang, Y. H. Zhang, X. D. Song, G. Qin and X. S. Zheng, *J. Electrochem. Soc.*, 166 (2019) E453.
26. J. H. Rong and Q. Q. Liang, *Comput. Meth. Appl. Mech. Eng.*, 197 (2008) 1447.
27. C. Madore, O. Piotrowski and D. Landolt, *J. Electrochem. Soc.*, 146 (1999) 2526.
28. M. Hackert-Oschätzchen, N. Lehnert, A. Martin and A. Schubert, *IOP Conf. Series: Materials Science and Engineering*, 118 (2016) 012036.

© 2021 The Authors. Published by ESG (www.electrochemsci.org). This article is an open access article distributed under the terms and conditions of the Creative Commons Attribution license (<http://creativecommons.org/licenses/by/4.0/>).